REPORT SD-TR-82-012

(12)

Multimode Low Pressure CW Chemical Laser Performance Including Source Flow Effects

H. MIRELS
Aerophysics Laboratory
Laboratory Operations
The Aerospace Corporation
El Segundo, Calif. 90245

APPROVED FOR PUBLIC RELEASE;
DISTRIBUTION UNLIMITED

25 March 1982

Sponsored by

DEFENSE ADVANCED RESEARCH PROJECTS AGENCY (DOD)
DARPA Order No. 3646
Monitored by SD under Contract No. F04701-81-C-0082

SPACE DIVISION
AIR FORCE SYSTEMS COMMAND
Los Angeles Air Force Station
P.O. Box 92960, Worldway Postal Center
Los Angeles, Calif. 90009

This report was submitted by The Aerospace Corporation, El Segundo, CA 90245 under Contract No. F04701-81-C-0082 with the Space Division, Deputy for Technology, P.O. Box 92960, Worldway Postal Center, Los Angeles, CA 90009. It was reviewed and approved for The Aerospace Corporation by W. R. Warren, Jr., Director, Aerophysics Laboratory. Lieutenant Efren V. Fornoles, SD/YLVS, was the project officer for Technology. Dr. H. Allan Pike is the Program Director for the DARPA Washington Office. This research was supported by the Defense Advanced Research Projects Agency of the Department of Defense.

This report has been reviewed by the Public Affairs Office (PAS) and is releasable to the National Technical Information Service (NTIS). At NTIS, it will be available to the general public, including foreign nations.

This technical report has been reviewed and is approved for publication. Publication of this report does not constitute Air Force approval of the report's findings or conclusions. It is published only for the exchange and stimulation of ideas.

Efren V. Fornoles
Efren V. Fornoles, 2nd Lt, USAF
Project Officer

Florian P. Meinhardt
Florian P. Meinhardt, Lt Col, USAF
Director, Directorate of Advanced
Space Development

FOR THE COMMANDER

Norman W. Lee
Norman W. Lee, Jr., Colonel, USAF
Deputy for Technology

UNCLASSIFIED

SECURITY CLASSIFICATION OF THIS PAGE (When Data Entered)

REPORT DOCUMENTATION PAGE		READ INSTRUCTIONS BEFORE COMPLETING FORM
1. REPORT NUMBER SD-TR-82-012	2. GOVT ACCESSION NO. AD-A114 473	3. RECIPIENT'S CATALOG NUMBER
4. TITLE (and Subtitle) MULTIMODE LOW PRESSURE CW CHEMICAL LASER PERFORMANCE INCLUDING SOURCE FLOW EFFECTS		5. TYPE OF REPORT & PERIOD COVERED
		6. PERFORMING ORG. REPORT NUMBER TR-0082(2764)-2
7. AUTHOR(s) Harold Mirels		8. CONTRACT OR GRANT NUMBER(s) F04701-81-C-0082
9. PERFORMING ORGANIZATION NAME AND ADDRESS The Aerospace Corporation El Segundo, Calif. 90245		10. PROGRAM ELEMENT, PROJECT, TASK AREA & WORK UNIT NUMBERS
11. CONTROLLING OFFICE NAME AND ADDRESS Defense Advanced Research Projects Agency 1400 Wilson Blvd. Arlington, Va. 22209		12. REPORT DATE 25 March 1982 13. NUMBER OF PAGES 47
14. MONITORING AGENCY NAME & ADDRESS(if different from Controlling Office) Space Division Air Force Systems Command Los Angeles, Calif. 90009		15. SECURITY CLASS. (of this report) Unclassified 15a. DECLASSIFICATION/DOWNGRADING SCHEDULE

16. DISTRIBUTION STATEMENT (of this Report)

Approved for public release; distribution unlimited.

17. DISTRIBUTION STATEMENT (of the abstract entered in Block 20, if different from Report)

18. SUPPLEMENTARY NOTES

19. KEY WORDS (Continue on reverse side if necessary and identify by block number)

Chemical Laser
Inhomogeneous Broadening
Multimode Operation
Source Flow

20. ABSTRACT (Continue on reverse side if necessary and identify by block number)

The performance of low pressure (inhomogeneously broadened) multiple longitudinal mode cw chemical lasers is investigated in the limit $\Delta\nu_c \ll \Delta\nu_h$, $\Delta\nu_h \ll \Delta\nu_d$ where $\Delta\nu_c$, $\Delta\nu_h$, and $\Delta\nu_d$ represent longitudinal mode separation, homogeneous width, and Doppler width, respectively. Effects of source flow (i.e., mean motion in optical path direction) are included. The present approach, in which power on spectral lineshape is assumed a priori, yields physically realistic, self consistent solutions for laser flow regimes of

DD FORM 1473 (FACSIMILE)

UNCLASSIFIED

SECURITY CLASSIFICATION OF THIS PAGE (When Data Entered)

19. KEY WORDS (Continued)

20. ABSTRACT (Continued)

practical interest. Numerical results, as well as analytic limit solutions, are provided. The decrement in net laser output power, caused by lack of saturation and by source flow, is evaluated. It is concluded that the latter can be estimated from numerical codes in which a single longitudinal mode is assumed at line center for each lasing transition, provided zero power line center gain is corrected for the source flow effect. It is also concluded that a limit solution deduced herein provides relatively accurate simple-closed-form analytic expressions for laser performance in the regime of interest.

CONTENTS

FIGURES

FIGURES (Continued)

TABLES

I. INTRODUCTION

The reaction zone in cw chemical lasers [Fig. 1(a)] is generally maintained at pressures of the order of 1 to 10 Torr to permit fast mixing of the reactants. At these pressures, the spectral lineshape is inhomogeneously broadened, i.e., the radiation field interacts with only a portion of the excited molecules. As a result, hole burning[1] may occur as the degree of optical saturation is increased. Hole burning affects laser output power and the index of refraction of the lasing medium.

A comprehensive theory for inhomogeneous broadening effects in a steady-state laser oscillator has been developed by Lamb.[2] Lamb's theory was generalized in Ref. 3 to account for effects of cross relaxation and streamwise flow variations in cw chemical lasers. Results were obtained for the case of a Fabry-Perot (F-P) resonator with a single longitudinal mode. The single longitudinal mode case corresponds to a mirror separation distance L [(Fig. 1(a)] up to approximately 1 m. For high-power lasers, the mirror separation can be of the order of 10 m, and many longitudinal modes are excited. The latter case was treated in Ref. 4 in the limit $\Delta\nu_c \ll \Delta\nu_h$, $\Delta\nu_h \ll \Delta\nu_d$ where $\Delta\nu_h$ and $\Delta\nu_d$ are characteristic homogeneous and Doppler widths, respectively, and $\Delta\nu_c$ is the longitudinal mode spacing (Fig. 2). In Refs. 3 and 4, a simplified two-level model is used, and closed form solutions are obtained. A numerical code developed by Bullock and Lipkis[5] treats the full system of equations that describe inhomogeneous broadening effects in cw chemical lasers. Results from Refs. 4 and 5 are in agreement in those regimes where both are applicable.[4]

Transverse flow expansion (i.e., source flow) can be used in cw chemical lasers[6] to reduce the temperature increase in the lasing region. The resulting mean motion in the optical path direction (e.g., Fig. 3) modifies the spectral lineshape of the lasing medium. The effect of source flow on a Doppler broadened lineshape is deduced in Ref. 6 for the case of small lateral motion and in Ref. 7 for the case of arbitrary lateral motion.

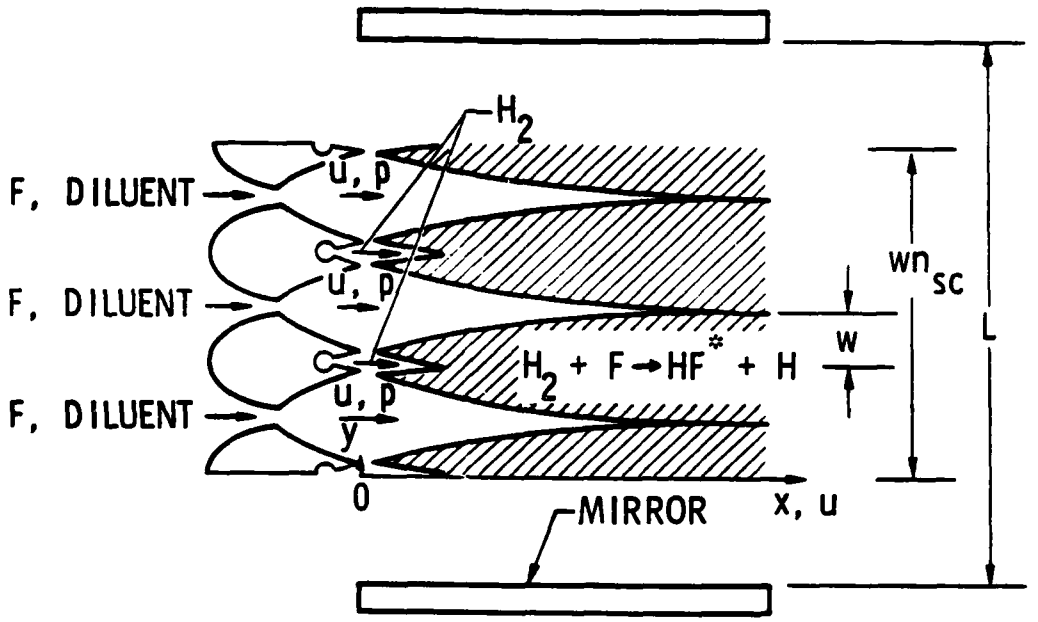

Figure 1(a). Continuous-wave chemical laser; flow field and F-P resonator

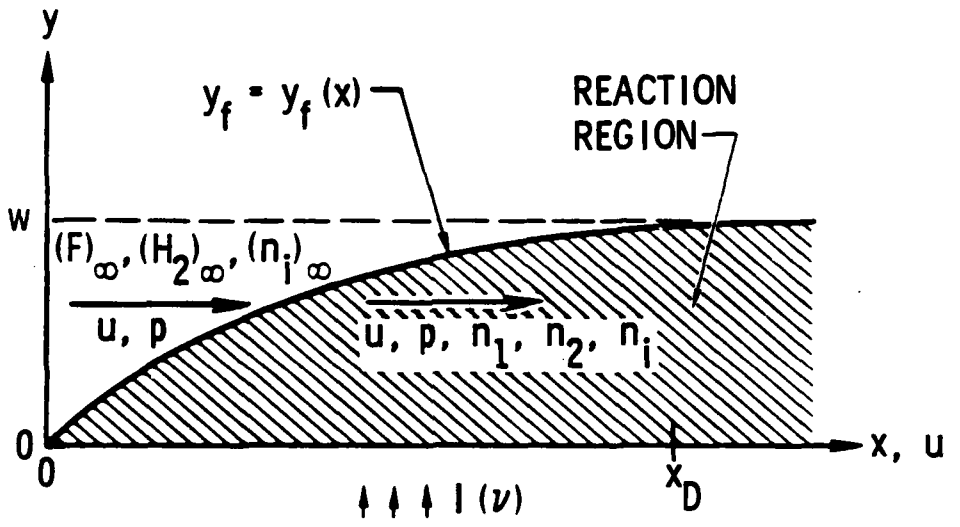

Figure 1(b). Continuous-wave chemical laser; flame sheet model of reaction zone

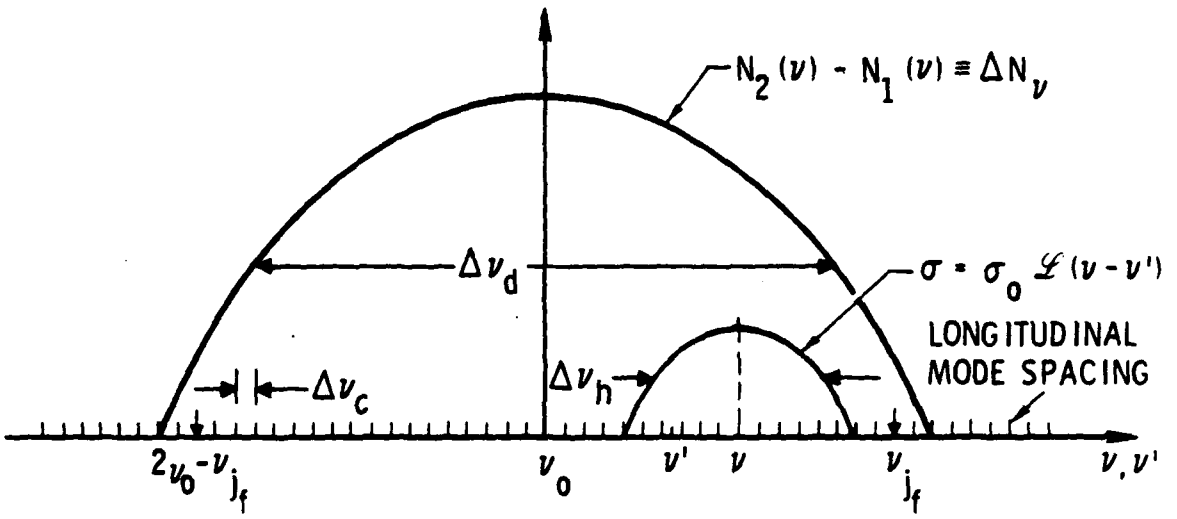

Figure 2(a). Characteristic frequencies and frequency-dependent variables for case $\Delta\nu_h \ll \Delta\nu_d$, $\Delta\nu_c \ll \Delta\nu_h$; nonlasing case

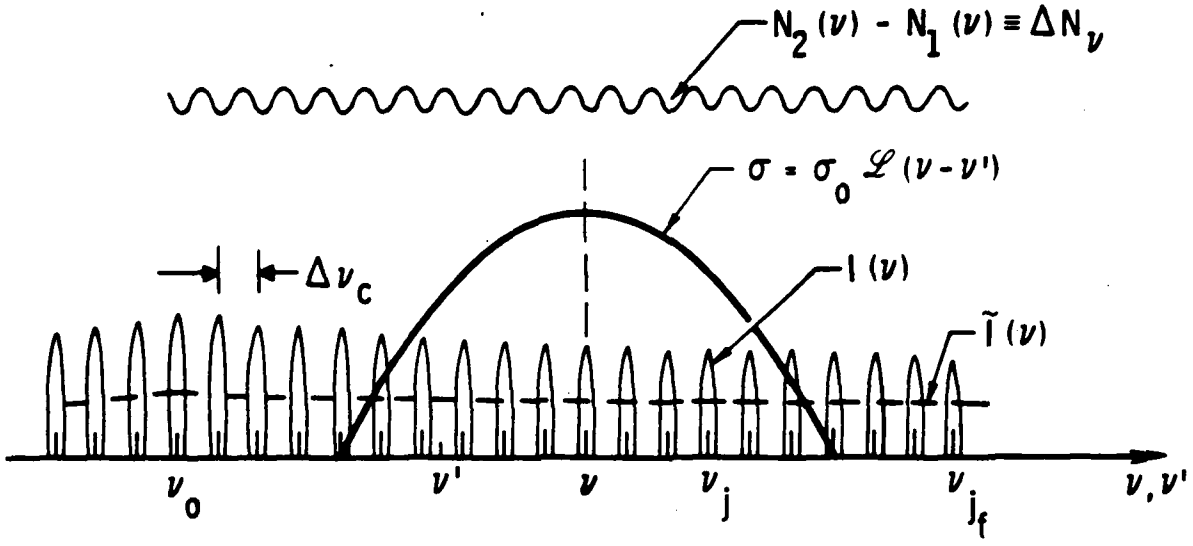

Figure 2(b). Characteristic frequencies and frequency-dependent variables for case $\Delta\nu_h \ll \Delta\nu_d$, $\Delta\nu_c \ll \Delta\nu_h$; lasing case

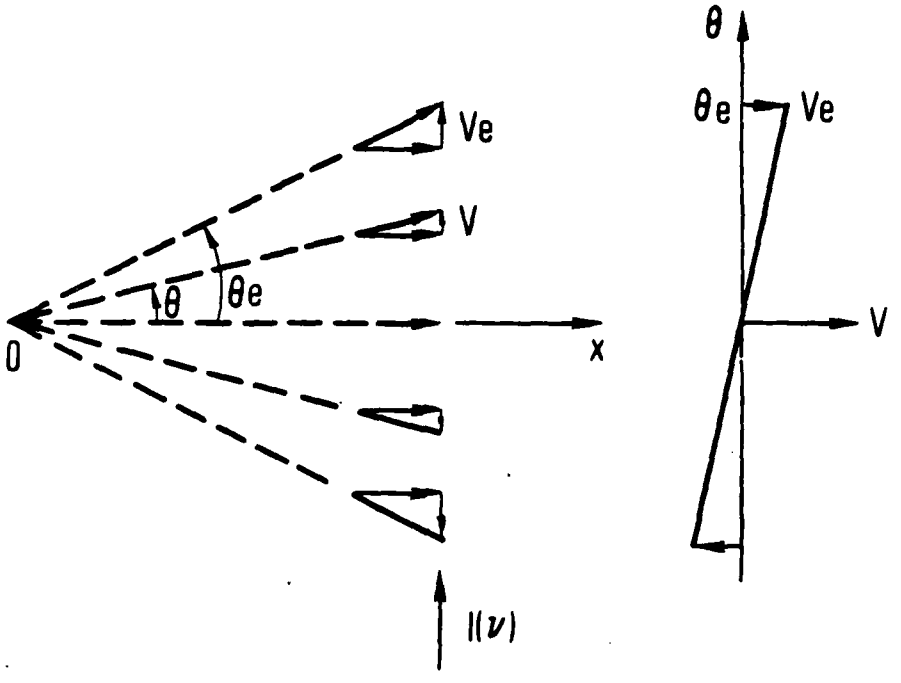

Figure 3. Source flow

In this report, the multiple longitudinal mode F-P resonator theory of Ref. 4 is modified to account for source flow effects. The primary objective is to evaluate the power decrement associated with source flow in cw chemical lasers. Numerical results are presented for cw chemical lasers with laminar diffusion.

II. THEORY

The model of Refs. 3 and 4 is generalized herein to include non-Maxwellian Doppler lineshapes. The performance of a multiple longitudinal mode cw chemical laser, including source flow effects, is then deduced. The development follows that in Ref. 4. Unless otherwise noted, the notation is the same as used in Ref. 4. Symbols are defined in Appendix A.

A. REGIME

It is assumed that

$$\Delta\nu_h \ll \Delta\nu_d \tag{1a}$$

$$\Delta\nu_c \ll \Delta\nu_h \tag{1b}$$

where $\Delta\nu_h$ and $\Delta\nu_d$ are characteristic homogeneous and Doppler widths, respectively, and $\Delta\nu_c$ is the longitudinal mode spacing, as illustrated in Figs. 2(a) and (2b). Expressions for these quantities are presented in Ref. 3. The inequality in Eq. (1a) is generally satisfied in cw chemical lasers and simplifies the relation between small signal gain and particle number density distribution.[3] Equation (1b) is used to simplify the effect of F-P resonator modes on lineshape.[4] The present results are believed valid[4] for $\Delta\nu_c/\Delta\nu_h \leq O(1)$. The latter inequality is satisfied for F-P mirror separation of the order of $L > O(10)$m.

B. MODEL

A cw HF chemical laser is illustrated in Fig. 1(a). The flame sheet model of Refs. 3 and 4 is illustrated in Fig. 1(b). The reactants are assumed to be premixed but do not react until a flame sheet $y_f(x)$ is reached. The form of the flame sheet is specified, a priori, from diffusion theory. The streamwise station where the flame sheet reaches the channel centerline, denoted x_D, characterizes the diffusion rate.

The reactants (e.g., H_2 + F) form upper vibrational level species at the flame sheet. Characteristic rates are normalized by the collisional deactivation rate k_{cd}. Streamwise distance is expressed in the form $\zeta = k_{cd}\, x/u$, which is the ratio of a convection time to a collisional deactivation time and is an order 1 quantity. The quantity $\zeta_D = k_{cd}\, x_D/u$ is the ratio of the diffusion time to the collisional deactivation time. It is assumed that $\zeta_D > \zeta_e$, where ζ_e denotes the station at which lasing is ended.

The difference between the net population, per unit volume, in the upper and lower lasing levels is expressed in normalized form as

$$\Delta N \equiv N_2 - N_1 = (n_2 - n_1)\, y_f/(n_r w) \tag{2a}$$

where n_r is a characteristic reactant number density upstream of the flame sheet, e.g., F_∞ in Fig. 1(b). Particles (per unit volume per unit frequency) resonant with laser frequencies in the range ν to $\nu + d\nu$ are denoted $n(\nu)$ and are normalized in the form

$$\Delta N_\nu \equiv N_2(\nu) - N_1(\nu) = [n_2(\nu) - n_1(\nu)]\, y_f/(n_r \bar{p}_o\, w) \tag{2b}$$

where

$$\bar{p}_o = [4\ (\ln 2)/\pi]^{1/2}/\Delta\nu_d \tag{2c}$$

The variation of ΔN_ν with ν is illustrated by Figs. 2(a) and 2(b) for nonlasing and lasing cases, respectively.[4]

The quantities ΔN and ΔN_ν are related by

$$\Delta N = \bar{p}_o \int_{-\infty}^{\infty} \Delta N_\nu\, d\nu \tag{3}$$

The normalized gain per unit length $G(\nu)$ equals

$$G(\nu) = \frac{g(\nu)\, y_f}{\sigma_o n_r w\, \bar{p}_o\, \Delta\nu_h} = \int_{-\infty}^{\infty} \mathscr{L}(\nu-\nu')\, \Delta N_{\nu'}\, \frac{d\nu'}{\Delta\nu_h} \tag{4a}$$

where $\mathscr{L}(\nu-\nu')$ is the Lorentzian (homogeneous lineshape)

$$\mathscr{L}(\nu-\nu') \equiv \frac{\sigma(\nu,\nu')}{\sigma_o} = \left[1 + 4\left(\frac{\nu-\nu'}{\Delta\nu_h}\right)^2\right]^{-1} \tag{4b}$$

The quantity $g(\nu)$ in Eq. (4a) is the gain per unit length in the reactive flow region $0 < y < y_f$ [Fig. 1(b)]. The average value of gain per unit length, including both reactive and nonreactive flow regions, is

$$g(\nu)_{av} = g(\nu)\, y_f/w \tag{4c}$$

Thus, the quantity $G(\nu)$ is seen to be a normalization of the average gain per unit length.

At this point, we depart from the development in Ref. 4 and assume a source flow with a linear variation of transverse velocities in the range $-V_e < V < V_e$ where V_e is the transverse velocity at the edge of the source flow (Fig. 3). In the absence of radiation, the particles have a distribution[7]

$$\frac{\Delta N_\nu}{\Delta N} = F(X, X_e) \tag{5a}$$

where

$$F(X,X_e) = \frac{\pi^{1/2}}{4X_e}\left[\operatorname{erf}(X + X_e) - \operatorname{erf}(X - X_e)\right] \tag{5b}$$

$$= e^{-X^2} \qquad (X_e = 0) \tag{5c}$$

$$= (\pi^{1/2}/2X_e)\ \text{erf}\ X_e \qquad (X = 0) \tag{5d}$$

$$X = 2\ (\ln 2)^{1/2}\ (\nu - \nu_o)/\Delta\nu_d \tag{5e}$$

$$X_e = V_e/a \tag{5f}$$

The function $F(X,X_e)$ is normalized such that

$$(2/\pi^{1/2}) \int_{-\infty}^{\infty} F(X,X_e)\ dX = 1 \tag{5g}$$

The quantity X_e is the ratio of maximum transverse velocity V_e to the most probable particle thermal speed a and is a measure of the importance of the transverse motion relative to thermal motion. Note that $F(X,X_e)$ is Maxwellian when $X_e = 0$. In the Doppler approximation ($\Delta\nu_h \ll \Delta\nu_d$) , the zero power gain equals

$$G(\nu) = (\pi/2)\ \Delta N_\nu = (\pi/2)\ \Delta N\ F(X,X_e) \tag{6}$$

which is illustrated in Fig. 4(a). Line center gain is decreased and frequency width is increased as X_e increases. If we let ν_j denote the center frequency for each longitudinal mode in an F-P resonator [Fig. 2(b)], the gain equal loss condition, for each mode, can be expressed[4]

$$G(\nu_j) \equiv G_c = \frac{(-1)\ (\ln R_m)/(w\ n_{sc})}{\sigma_o\ n_r\ \Delta\nu_h\ \bar{P}_o} \tag{7a}$$

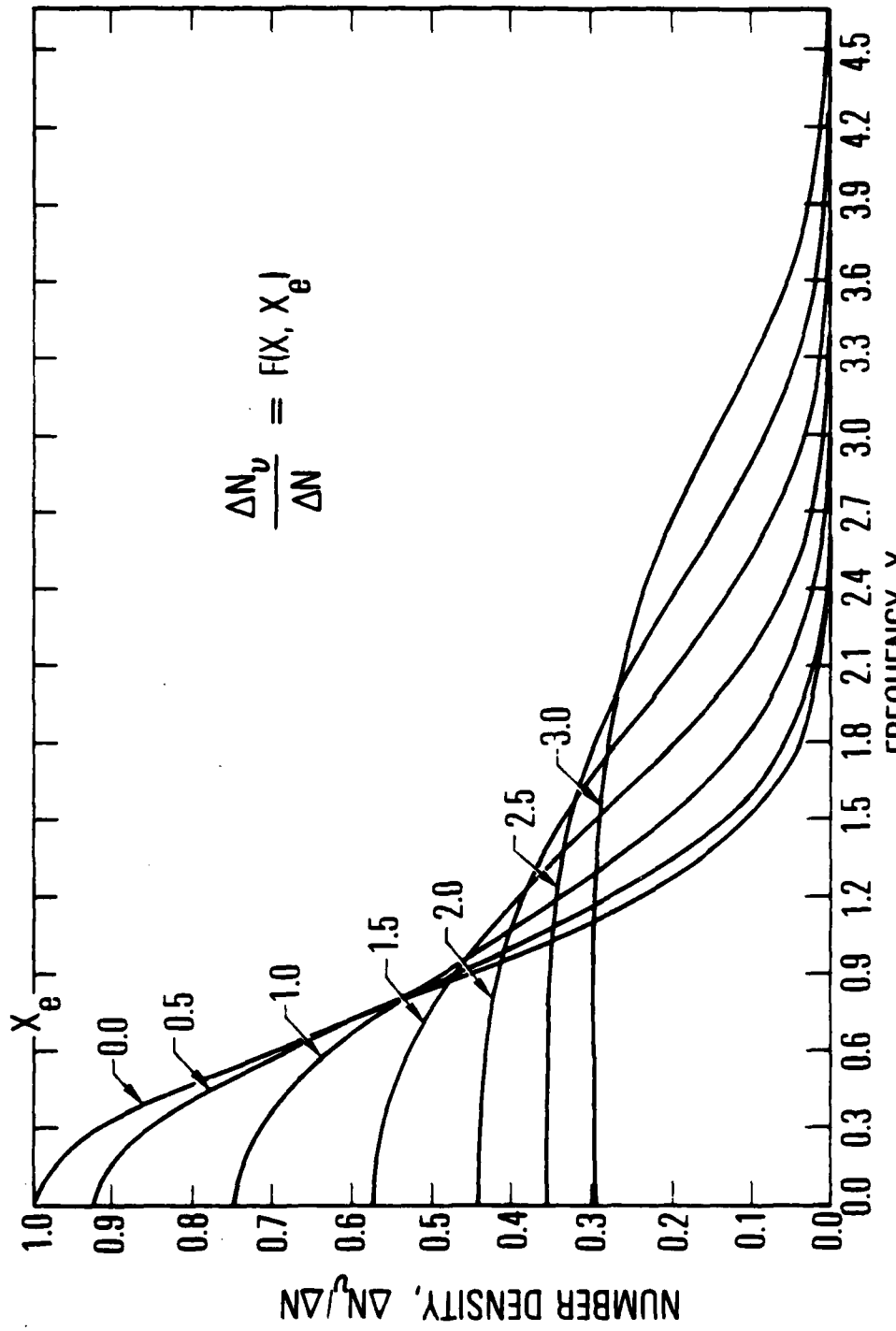

Figure 4(a). Variation of number density with frequency at two streamwise stations; upstream of lasing region, $\zeta < \zeta_1$

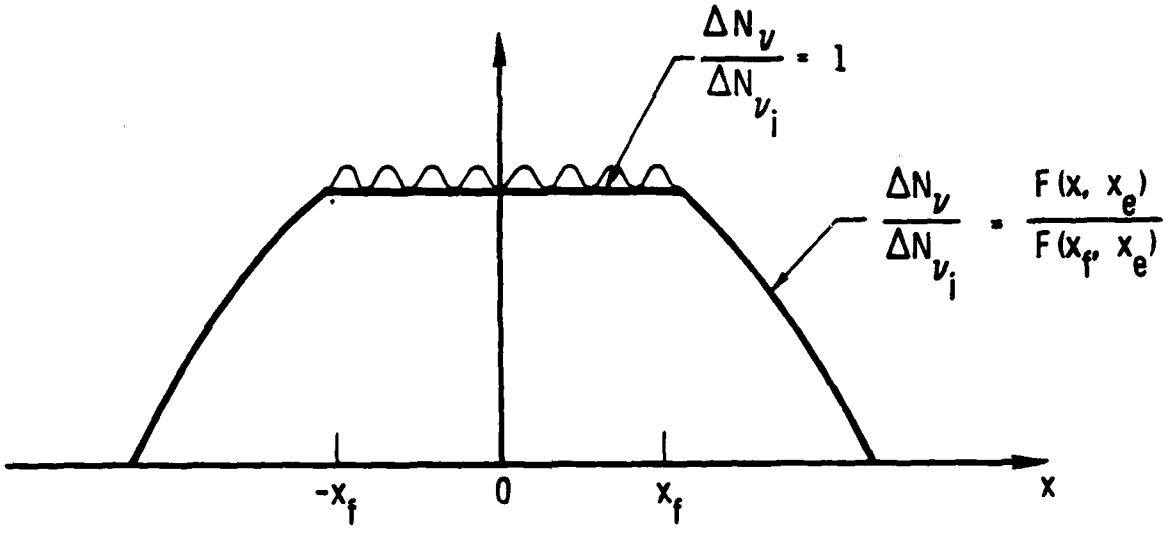

Figure 4(b). Variation of number density with frequency at two streamwise stations; in lasing region $\zeta > \zeta_i$

where R_m is the reflectivity of one mirror and $n_{sc}w$ is the net width of the gain region [Fig. 1(a)]. Equation (7a) follows from the average value of gain, under threshold conditions in an F-P resonator, i.e.,

$$(g_c)_{av} = (-1)(\ln R_m)/(wn_{sc}) \tag{7b}$$

For convenience, the mirror separation L is assumed to permit a longitudinal mode at ν_o. Lasing is initiated at the streamwise station where $G(\nu_o) = G_c$. If we let ΔN_i denote the value of ΔN and ΔN_{ν_i} denote the line center ($X = 0$) value of ΔN_ν at the station where lasing is initiated, these quantities are related by

$$(2/\pi)\, G_c = \Delta N_{\nu_i} = \Delta N_i\, F(0,X_e) \tag{8}$$

Equation (8) defines upstream boundary conditions for the lasing region.

In view of Eq. (1b), the spectral lineshape under laser conditions can be assumed to have the form [Fig. 4(b)]

$$\frac{\Delta N_\nu}{\Delta N_{\nu_i}} = 1 \qquad |X| < X_f \tag{9a}$$

$$= \frac{F(X,X_e)}{F(X_f,X_e)} \qquad |X| > X_f \tag{9b}$$

where X_f is the value of X corresponding to the largest lasing frequency and $|X| < X_f$ denotes the lasing region. In Eq. (9a), small departures from 1 in the lasing region are neglected [e.g., Figs. 2(b) and 4(b)].

If we let

$$\frac{\Delta N}{\Delta N_{\nu_i}} = H(X_f, X_e) \tag{10a}$$

substitution of Eq. (9) into Eq. (3) yields

$$H(X_f, X_e) \equiv \frac{2}{\pi^{1/2}} \left[X_f + \frac{1}{F(X_f, X_e)} \int_{X_f}^{\infty} F(X, X_e)\, dX \right] \tag{10b}$$

$$= \frac{2}{\pi^{1/2}} X_f + \frac{1}{2X_e F(X_f, X_e)} \left\{ \frac{1}{\pi^{1/2}} \left[e^{-(X_f - X_e)^2} - e^{-(X_f + X_e)^2} \right] \right.$$

$$\left. + (X_f + X_e)\, \mathrm{erfc}\, (X_f + X_e) - (X_f - X_e)\, \mathrm{erfc}\, (X_f - X_e) \right\} \tag{10c}$$

$$= \frac{2}{\pi^{1/2}} X_f + e^{X_f^2}\, \mathrm{erfc}\, X_f \qquad (X_e = 0) \tag{10d}$$

$$= 1/F(0, X_e) \qquad (X_f = 0) \tag{10e}$$

The quantities X_f and ΔN are functions of streamwise distance, which are evaluated in the course of the solution.

C. LASER PERFORMANCE

The variation of ΔN_ν and ΔN with normalized streamwise distance ζ was deduced in Ref. 4 for the case of a Maxwellian zero power lineshape e^{-X^2}. These equations are applicable in the present study if e^{-X^2} is replaced by $F(X, X_e)$. Equations (12a) and (12b) of Ref. 4 then become

$$\frac{d\Delta N_\nu}{d\zeta} = F(X,X_e)\ \left[(dN_T/d\zeta) - N_T + R\Delta N\right]$$

$$- (1+R)\ \Delta N_\nu - \pi\ \Delta\nu_h\ \Delta N_\nu\ \tilde{I}(\nu) \qquad (11a)$$

$$\frac{d\Delta N}{d\zeta} = \frac{dN_T}{d\zeta} - N_T - \Delta N - 2\ \frac{dP}{d\zeta} \qquad (11b)$$

where

$$\frac{dP}{d\zeta} \equiv \frac{2}{\pi^{1/2}}\ \Delta\nu_h \int_0^{X_f} G_c\ \tilde{I}\ dX \qquad (11c)$$

Effects of chemical pumping, collisional deactivation, cross relaxation (velocity exchanging collisions) and stimulated emission and absorption as discussed in Ref. 4 are included in Eqs. (11a) through (11c). Here $N_T = N_1 + N_2$, $R = k_{cr}/k_{cd}$ = cross relaxation rate/collisional deactivation rate, P = normalized output power extracted up to station ζ, and $\tilde{I}(\nu)$ represents a continuous intensity distribution, which replaces the discrete intensity distribution I_j [i.e., $\tilde{I}(\nu) = I_j/\Delta\nu_c$] in accord with the approximation $\Delta\nu_c \ll \Delta\nu_h$. The cross relaxation parameter R, which can be viewed as the number of collisions required to deactivate an excited particle, is of the order 10 to 100 for an HF laser.[3]

The variation of X_f with ζ can be found by consideration of Eq. (11a) in the region $|X| > X_f$, $\tilde{I} = 0$. Substitution of Eq. (5b) into Eq. (11a), with $\tilde{I} = 0$, yields

$$\frac{(-1)\left[dF(X_f,X_e)/dX_f^2\right]}{\left[F(X_f,X_e)\right]^2}\ \frac{dX_f^2}{d\zeta} = \frac{1}{\Delta N_{\nu_i}}\left(\frac{dN_T}{d\zeta} - N_T\right) + RH(X_f,X_e)$$

$$- \frac{(1+R)}{F(X_f,X_e)} \qquad (12a)$$

where H is as defined in Eq. (10b) and, from Eq. (5b)

$$\frac{dF(X_f,X_e)}{dX_f^2} = \frac{(-1)}{4\,X_e X_f}\left[e^{-(X_f-X_e)^2} - e^{-(X_f+X_e)^2}\right]$$

The initial condition for Eq. (12a) is

$$X_f = 0 \text{ at } \zeta = \zeta_i \tag{12b}$$

where ζ_i is the station at which lasing is initiated. The use of X_f^2 as the dependent variable in Eq. (12a) avoids singular behavior near ζ_i. Equations (12a) and (12b) can be integrated to provide X_f as a function of ζ if $N_T/\Delta N_{\nu_i}$ is specified. The magnitude of X_f increases, reaches a maximum, and then decreases as ζ is increased. The corresponding variation of $\Delta N/\Delta N_{\nu_i}$ with ζ is then found from Eq. (10).

The lasing intensity $\tilde{I}$ is evaluated by consideration of Eq. (11a) in the region $|X| \leq X_f$, $d\Delta N_\nu/d\zeta = 0$. Substitution of the latter into Eq. (11a) yields

$$\frac{\pi\,\Delta\nu_h\,\tilde{I} + 1 + R}{F(X,X_e)} = \frac{1}{\Delta N_{\nu_i}}\left(\frac{dN_T}{d\zeta} - N_T\right) + RH(X_f,X_e) \tag{13a}$$

The right hand side of Eq. (13a) is independent of X. Hence, at each streamwise station, $\pi\,\Delta\nu_h\,\tilde{I}$ is equal to a term proportional to $F(X,X_e)$ minus the quantity $(1 + R)$. At some streamwise stations, $\tilde{I}$ is negative in the vicinity of $X = X_f$. Conditions under which $\tilde{I}$ is negative can be deduced from

$$\frac{\pi \Delta\nu_h \tilde{I}}{F(X,X_e)} = \frac{(-1)}{[F(X_f,X_e)]^2} \frac{dF(X_f,X_e)}{dX_f^2} \frac{dX_f^2}{d\zeta}$$

$$+ (1+R)\left[\frac{F(X,X_e) - F(X_f,X_e)}{F(X,X_e)\, F(X_f,X_e)}\right] \tag{13b}$$

which follows from Eqs. (1a) and (13a). The coefficients of $dX_f^2/d\zeta$ and $1 + R$ in Eq. (13b) are positive quantities. Hence $\tilde{I}$ is positive for all $|X| \leq X_f$ when $dX_f^2/d\zeta$ is nonnegative. At downstream stations where $dX_f^2/d\zeta$ is negative, $\tilde{I}$ becomes negative in the vicinity of $X = X_f$. The extent of the negative $\tilde{I}$ region depends on the magnitude of R (i.e., the larger the magnitude of R is, the smaller is the extent of the negative region).

Negative values of $\tilde{I}$ correspond to power absorption by the lasing medium [Eq. (11c)]. The absorption is needed at downstream stations ($dX_f^2/d\zeta < 0$) to maintain the constant gain boundary condition [Eq. (7a)] for longitudinal modes near $X = X_f$. Negative values of $\tilde{I}$ are unrealistic and arise at the downstream stations because of the a priori choice of lineshape in the region $|X| > X_f$. The present solution is valid for those cases where negative values of $\tilde{I}$ are absent or negligible. The net power liberated up to station ζ is, from Eq. (11b)

$$\frac{2P}{\Delta N_{\nu_i}} = \left[\frac{N_T}{\Delta N_{\nu_i}} - H(X_f,X_e)\right]_{\zeta_i}^{\zeta} - \int_{\zeta_i}^{\zeta} \left[\frac{N_T}{\Delta N_{\nu_i}} + H(X_f,X_e)\right] d\zeta \tag{14}$$

A similar expression, deduced from Eqs. (11c) and (13), indicates the self consistency of the present solution. The total output power from the laser P_e is found by evaluation of the upper limit in Eq. (14) at the station ζ_e where $dP/d\zeta = 0$ [Eq. (11b)].

The performance of a cw chemical laser, including source flow effects, is defined by Eqs. (12) through (14).

D. LAMINAR DIFFUSION

We now consider the case in which the flame sheet in Fig. 1(b) corresponds to laminar diffusion. Arbitrary values of the parameters R and G_c are considered, and analytic solutions are then obtained for limiting cases.

For laminar diffusion, the flame sheet has the form

$$y_f/w = (x/x_D)^{1/2} \tag{15}$$

and N_T is approximated by[3,4]

$$\zeta_D^{1/2} N_T = \zeta^{1/2} \tag{16}$$

The rate of chemical pumping is defined by Eq. (16), in which it is assumed that the pumping reaction goes to completion at the flame sheet. Equations (12) through (14) can now be solved.

1. ZERO POWER ($\zeta < \zeta_i$)

Integration of Eq. (11b) in the absence of lasing and substitution of Eq. (6) yields

$$\zeta_D^{1/2} \Delta N = (2/\pi)\, \zeta_D^{1/2}\, G(\nu)/F(X,X_e) = 2D(\zeta^{1/2}) - \zeta^{1/2} \tag{17a}$$

where D ( ) is the Dawson integral

$$D(X) = e^{-X^2} \int_o^X e^{X_o^2}\, dX_o \tag{17b}$$

In the absence of lasing, the net inversion ΔN is independent of X_e, whereas the gain $G(\nu)$ depends on X_e. The quantity ΔN reaches a maximum at $\zeta = 0.3051$. At this station,

$$\zeta_D^{1/2} \, \Delta N_{mzp} = 0.3528 \tag{18}$$

where subscript mzp denotes maximum zero power value. Equation (18) can be used to convert normalized variables to physical variables for cases where the maximum zero power value of average line center gain for the case $X_e = 0$, which is denoted by g_{mzp}, has been evaluated numerically or experimentally. Then, from Eqs. (4a) and (18)

$$\sigma_o \, n_r \, \bar{p}_o \, \Delta\nu_h / \zeta_D^{1/2} = 1.804 \, g_{mzp} \tag{19a}$$

$$(g_c)_{av} / g_{mzp} = 1.804 \, \zeta_D^{1/2} \, G_c \tag{19b}$$

where $1.804 = (2/\pi)/0.3528$ and

$$g_{mzp} \equiv \left\{ [g(\nu_o)]_{av}, \; X_e = 0 \right\}_{mzp}$$

Equations (19a) and (19b) apply for the case of a laminar diffusion flame if $\zeta_D > 0.3051$.

The zero power gain decreases to zero at $\zeta = 1.1301$, so lasing is restricted to the region $0 < \zeta < 1.1301$. Lasing is initiated at the station where the threshold gain is reached. Thus,

$$\zeta_D^{1/2}\ \Delta N_i = \tilde{G}_c = 2D\left(\zeta_i^{1/2}\right) - \zeta_i^{1/2} \tag{20a}$$

where

$$\tilde{G}_c = \frac{2}{\pi}\ \frac{\zeta_D^{1/2}\ G_c}{F(0,X_e)} \tag{20b}$$

For a given value of $\tilde{G}_c$, ζ_i is obtained from Eq. (20a) by iteration and must lie in the range $0 < \zeta_i < 0.3051$. Note, from Eqs. (18) and (20), that $\tilde{G}_c < 0.3528$. The laser is saturated when $\tilde{G}_c/0.3528 \ll 1$. In this region

$$\zeta_i^{1/2} = \tilde{G}_c \left[1 + (4/3)\ \tilde{G}_c^2 + 0\ \left(\tilde{G}_c^4\right)\right] \tag{20c}$$

2. POWER ON ($\zeta > \zeta_i$)

The variation of X_f with ζ in the lasing region $\zeta > \zeta_i$ is found by substitution of Eq. (16) into Eq. (12). The result is

$$\frac{dX_f^2}{dZ} = \frac{[F(X_f,X_e)]^2}{(-1)\ dF/dX_f^2}\left[\frac{1 - 2Z^2}{\tilde{G}_c\ F(0,X_e)} + 2ZRH(X_f,X_e) - \frac{2Z\ (1+R)}{F(X_f,X_e)}\right] \tag{21a}$$

with boundary conditions

$$X_f = 0 \text{ at } Z = Z_i \tag{21b}$$

where $Z = \zeta^{1/2}$. The variables are taken to be X_f^2 and Z in Eq. (21), to avoid a singularity at Z_i. At Z_i, Eq. (21a) becomes

$$\frac{dX_f^2}{dZ} = \frac{X_e^2}{\tilde{G}_c\, F(0,X_e)} \left(1 - 2Z_i^2 - 2Z_i\, \tilde{G}_c\right) \tag{22}$$

which is independent of R. A numerical integration of Eq. (21) is generally required.

The intensity distribution is obtained from

$$\frac{\pi\, \Delta\nu_h\, \tilde{I} + 1+R}{F(X,X_e)} = \frac{1}{\tilde{G}_c\, F(0,X_e)} \left(\frac{1}{2Z} - Z\right) + RH(X_f,X_e) \tag{23}$$

The output power to station Z equals, from Eq. (14),

$$2\zeta_D^{1/2}\, P = \left[Z - \frac{2}{3} Z^3 - \tilde{G}_c\, F(0,X_e)\, H(X_f,X_e)\right]_{Z_i}^{Z}$$

$$- 2\, \tilde{G}_c\, F(0,X_e) \int_{Z_i}^{Z} Z\, H(X_f,X_e)\, dZ \tag{24}$$

Numerical results, presented in Tables I through III and Figs. 5 through 7, are discussed in Section III.

3. LIMIT $R \gg 1$, $R\tilde{G}_c \gg 1$

The limit $R \gg 1$, $R\, \tilde{G}_c \gg 1$ is now considered. It is clear from physical considerations that X_f decreases as R and $\tilde{G}_c$ increase. The present limits ensure that terms of order X_f^2 can be neglected compared to 1.

Table I. Station at which lasing is initiated[a]

	z_i					
$\frac{2}{\pi}\zeta_D^{1/2}G_c$	$X_e = 0.001$	$X_e = 0.5$	$X_e = 1.0$	$X_e = 1.5$	$X_e = 2.0$	$X_e = 2.5$
3.530^{-3}	3.530^{-3}	3.826^{-3}	4.727^{-3}	6.185^{-3}	8.004^{-3}	9.963^{-3}
7.060^{-3}	7.060^{-3}	7.653^{-3}	9.454^{-3}	1.237^{-2}	1.601^{-2}	1.993^{-2}
1.765^{-2}	1.766^{-2}	1.914^{-2}	2.365^{-2}	3.096^{-2}	4.010^{-2}	4.998^{-2}
3.530^{-2}	3.536^{-2}	3.834^{-2}	4.741^{-2}	6.216^{-2}	8.074^{-2}	1.010^{-1}
7.060^{-2}	7.108^{-2}	7.714^{-2}	9.570^{-2}	1.264^{-1}	1.661^{-1}	2.117^{-1}

[a]Superscript denotes exponent of ten (e.g., $3.530^{-3} = 3.530 \times 10^{-3}$).

Table II. Station at which $dP/d\zeta = 0$ and corresponding laser output power

$\frac{\pi}{2}\zeta_D^{1/2}G_c(a)$	R	$X_e = 0.001$		$X_e = 0.5$		$X_e = 1.0$		$X_e = 1.5$		$X_e = 2.0$		$X_e = 2.5$	
		Z_e	$\frac{P_e}{P_{e,s}}$	Z_e	$\frac{P_e}{P_{e,s}}$	Z_e	$\frac{P_e}{P_{e,s}}$	Z_e	$\frac{P_e}{P_{e,s}}$	Z_e	$\frac{P_e}{P_{e,s}}$	Z_e	$\frac{P_e}{P_{e,s}}$
3.530^{-3}	1	0.704	0.971	0.714	0.969	0.703	0.965	0.702	0.960	0.702	0.955	0.700	0.949
	10	0.710	0.978	0.710	0.976	0.709	0.972	0.710	0.968	0.708	0.963	0.706	0.957
	100	0.716	0.986	0.720	0.984	0.713	0.981	0.714	0.977	0.712	0.972	0.708	0.966
	1000	0.710	0.988	0.710	0.987	0.709	0.984	0.708	0.979	0.706	0.974	0.704	0.968
	∞	0.705	0.989	0.705	0.988	0.705	0.985	0.704	0.980	0.703	0.975	0.702	0.968
7.060^{-3}	1	0.701	0.947	0.698	0.943	0.700	0.935	0.698	0.926	0.696	0.915	0.694	0.904
	10	0.711	0.959	0.712	0.956	0.710	0.949	0.708	0.940	0.708	0.930	0.706	0.919
	100	0.715	0.973	0.722	0.971	0.716	0.965	0.712	0.956	0.710	0.945	0.706	0.933
	1000	0.709	0.976	0.710	0.974	0.708	0.969	0.706	0.959	0.704	0.948	0.700	0.936
	∞	0.704	0.978	0.703	0.976	0.702	0.970	0.701	0.961	0.699	0.949	0.697	0.937
1.765^{-2}	1	0.694	0.881	0.693	0.873	0.690	0.855	0.687	0.832	0.682	0.808	0.678	0.782
	10	0.714	0.910	0.713	0.904	0.714	0.887	0.709	0.865	0.704	0.840	0.698	0.814
	100	0.716	0.936	0.715	0.931	0.714	0.916	0.709	0.894	0.702	0.867	0.694	0.838
	1000	0.706	0.942	0.705	0.937	0.704	0.923	0.699	0.900	0.694	0.872	0.686	0.842
	∞	0.698	0.944	0.698	0.939	0.695	0.925	0.692	0.902	0.687	0.874	0.683	0.843
3.530^{-2}	1	0.683	0.787	0.680	0.773	0.677	0.740	0.674	0.697	0.663	0.651	0.655	0.602
	10	0.715	0.837	0.714	0.825	0.711	0.795	0.704	0.751	0.695	0.702	0.683	0.650
	100	0.711	0.877	0.710	0.867	0.707	0.839	0.698	0.795	0.687	0.741	0.673	0.684
	1000	0.699	0.886	0.698	0.876	0.693	0.848	0.686	0.804	0.677	0.748	0.665	0.690
	∞	0.690	0.889	0.688	0.879	0.684	0.851	0.677	0.806	0.668	0.750	0.659	0.691
7.060^{-2}	1	0.665	0.628	0.663	0.605	0.654	0.547	0.642	0.471	0.586	0.397	0.614	0.303
	10	0.711	0.704	0.709	0.684	0.704	0.626	0.688	0.544	0.668	0.450	0.648	0.352
	100	0.701	0.764	0.699	0.745	0.692	0.690	0.676	0.604	0.656	0.501	0.632	0.392
	1000	0.683	0.776	0.681	0.758	0.674	0.703	0.658	0.616	0.640	0.509	0.622	0.398
	∞	0.673	0.779	0.670	0.761	0.661	0.706	0.648	0.619	0.632	0.512	0.615	0.399

[a]Superscript denotes exponent of ten (e.g., $3.530^{-3} = 3.530 \times 10^{-3}$).

Table III. Downstream station at which $X_f = 0$ and corresponding output power

$\frac{\pi}{2}\zeta_D^{1/2}G_c$ (a)	R	$X_e = 0.001$		$X_e = 1.0$		$X_e = 2.0$	
		Z_L	$\frac{P_L}{P_{e,s}}$	Z_L	$\frac{P_L}{P_{e,s}}$	Z_L	$\frac{P_L}{P_{e,s}}$
3.530^{-3}	1	0.978	0.727	0.977	0.722	0.975	0.713
	10	0.786	0.964	0.786	0.957	0.783	0.949
	100	0.724	0.985	0.724	0.981	0.720	0.971
	1000	0.710	0.988	0.710	0.984	0.707	0.974
	∞	0.705	0.989	0.705	0.985	0.703	0.975
7.060^{-3}	1	0.977	0.706	0.977	0.696	0.972	0.677
	10	0.789	0.946	0.790	0.936	0.785	0.917
	100	0.724	0.973	0.725	0.965	0.718	0.945
	1000	0.710	0.976	0.709	0.969	0.704	0.948
	∞	0.704	0.978	0.701	0.970	0.699	0.949
1.765^{-2}	1	0.974	0.650	0.971	0.628	0.960	0.585
	10	0.795	0.898	0.795	0.875	0.784	0.827
	100	0.725	0.936	0.723	0.916	0.711	0.867
	1000	0.706	0.942	0.704	0.923	0.694	0.872
	∞	0.698	0.944	0.695	0.925	0.687	0.874
3.530^{-2}	1	0.966	0.572	0.960	0.531	0.937	0.454
	10	0.798	0.825	0.796	0.783	0.777	0.689
	100	0.720	0.877	0.716	0.839	0.696	0.741
	1000	0.700	0.886	0.693	0.848	0.677	0.748
	∞	0.690	0.889	0.684	0.851	0.668	0.750
7.060^{-2}	1	0.949	0.441	0.934	0.374	0.882	0.244
	10	0.796	0.693	0.790	0.615	0.753	0.437
	100	0.710	0.764	0.701	0.690	0.665	0.501
	1000	0.684	0.776	0.674	0.703	0.641	0.509
	∞	0.673	0.779	0.661	0.706	0.632	0.512

[a]Superscript denotes exponent of ten (e.g., $3.530^{-3} = 3.530 \times 10^{-3}$).

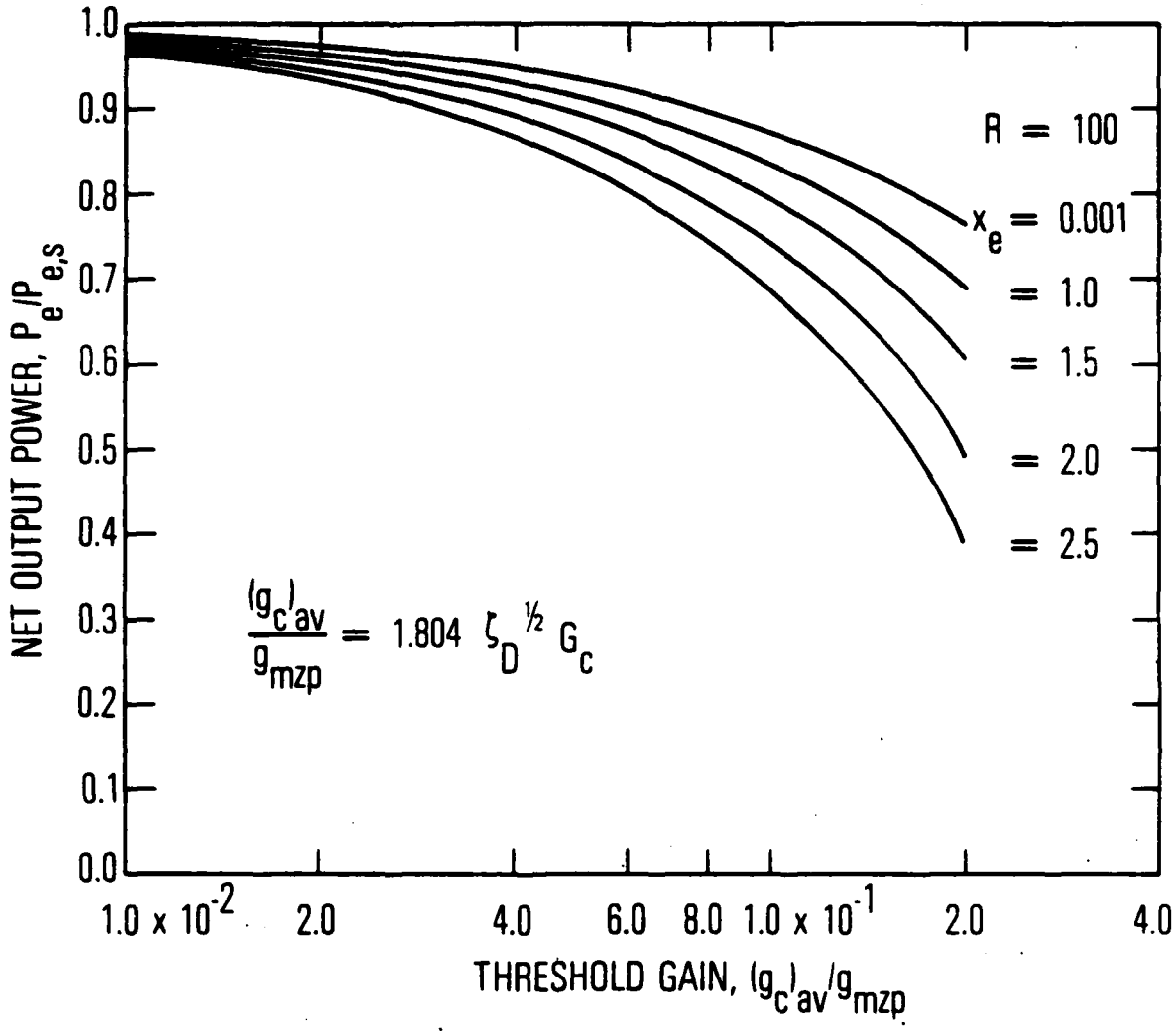

Figure 5. Effect of threshold gain parameter G_c and source flow parameter X_e on net output power for case of laminar flame sheet and R = 100

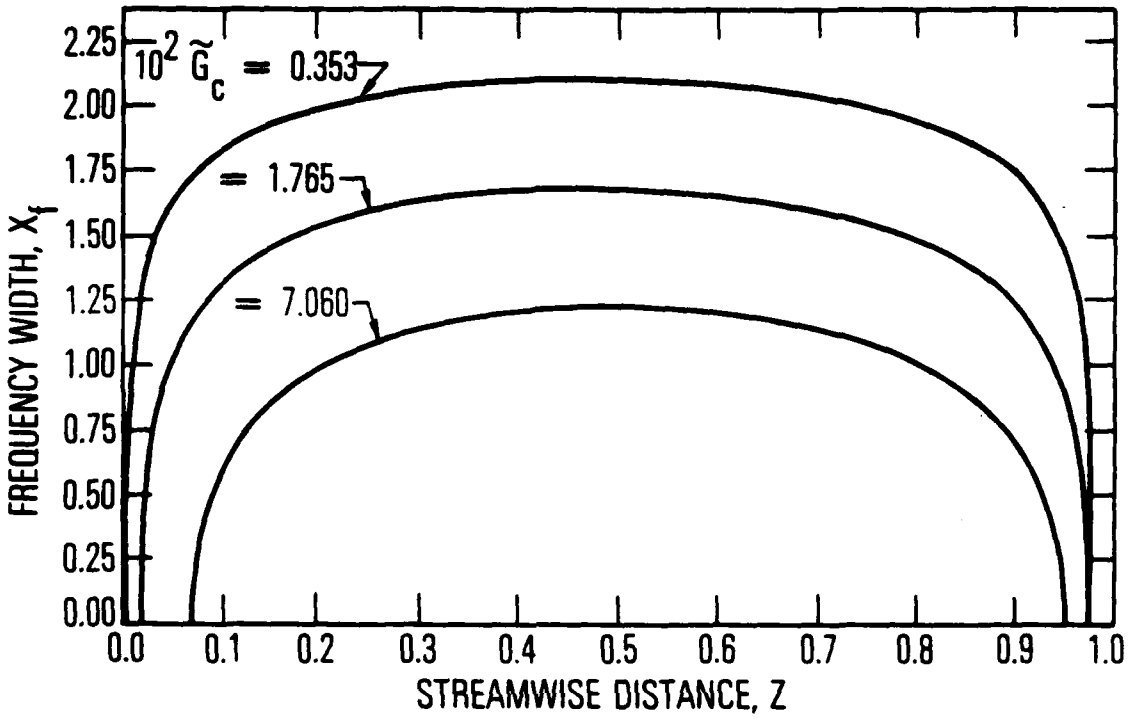

Figure 6(a). Numerical solution of Eqs. (10), (21), and (24) for case of laminar flame sheet R = 1, X_e = 0.001, and $10^2 \tilde{G}_c$ = 0.353, 1.765, 7.060; frequency width, X_f

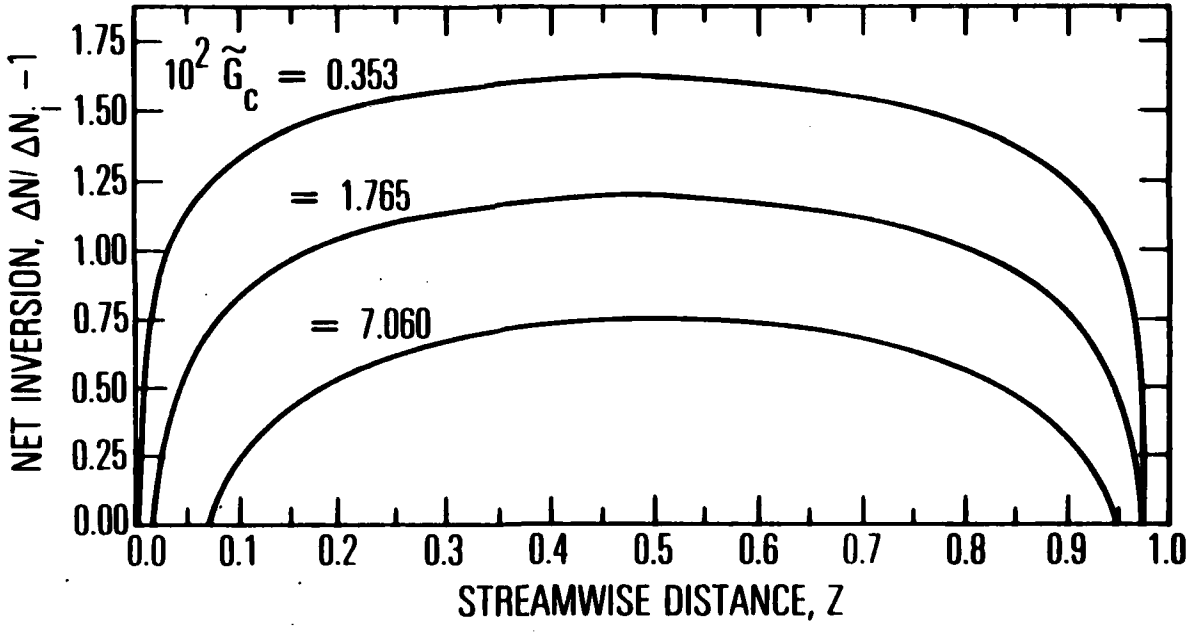

Figure 6(b). Numerical solution of Eqs. (10), (21), and (24) for case of laminar flame sheet R = 1, X_e = 0.001, and $10^2 \tilde{G}_c$ = 0.353, 1.765, 7.060; net inversion, $\Delta N/\Delta N_1$

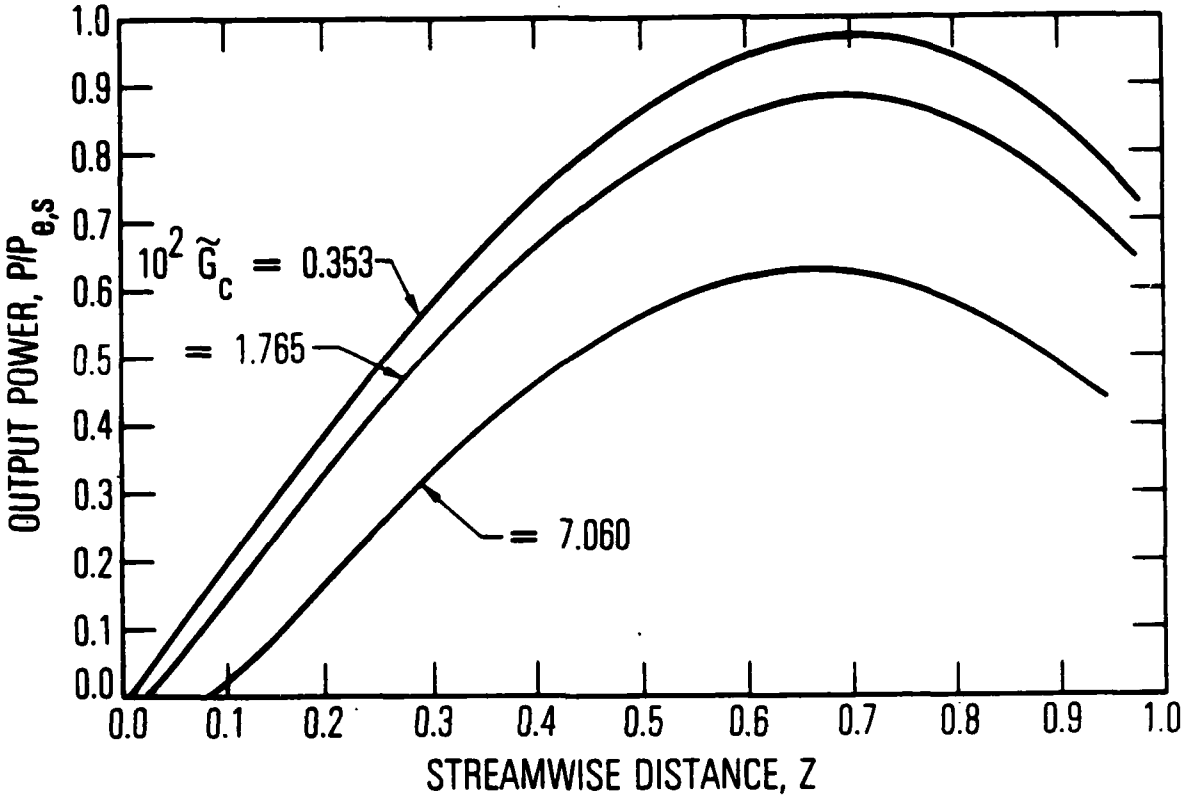

Figure 6(c). Numerical solution of Eqs. (10), (21), and (24) for case of laminar flame sheet R = 1, X_e = 0.001, and $10^2\,\tilde{G}_c$ = 0.353, 1.765, 7.060; output power, $P_e/P_{e,s}$

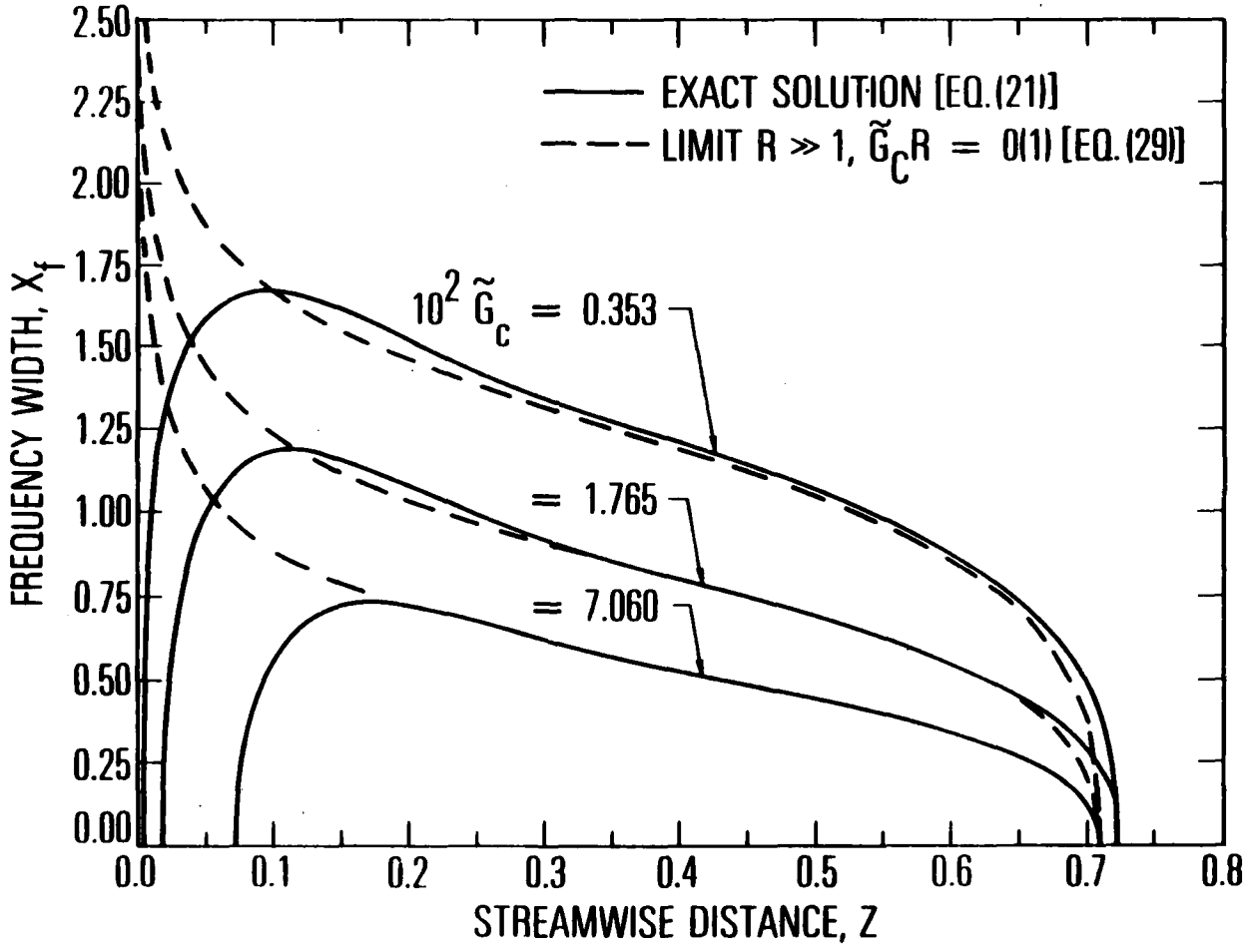

Figure 7(a). Numerical solutions of Eqs. (10), (21), and (24) for cage of laminar flame sheet R = 100, X_e = 0.001, and $10^2\,\tilde{G}_c$ = 0.353, 1.765, 7.060, including comparison with analytic solution in limit R >> 1, R $\tilde{G}_c$ = O(1); frequency width, X_f

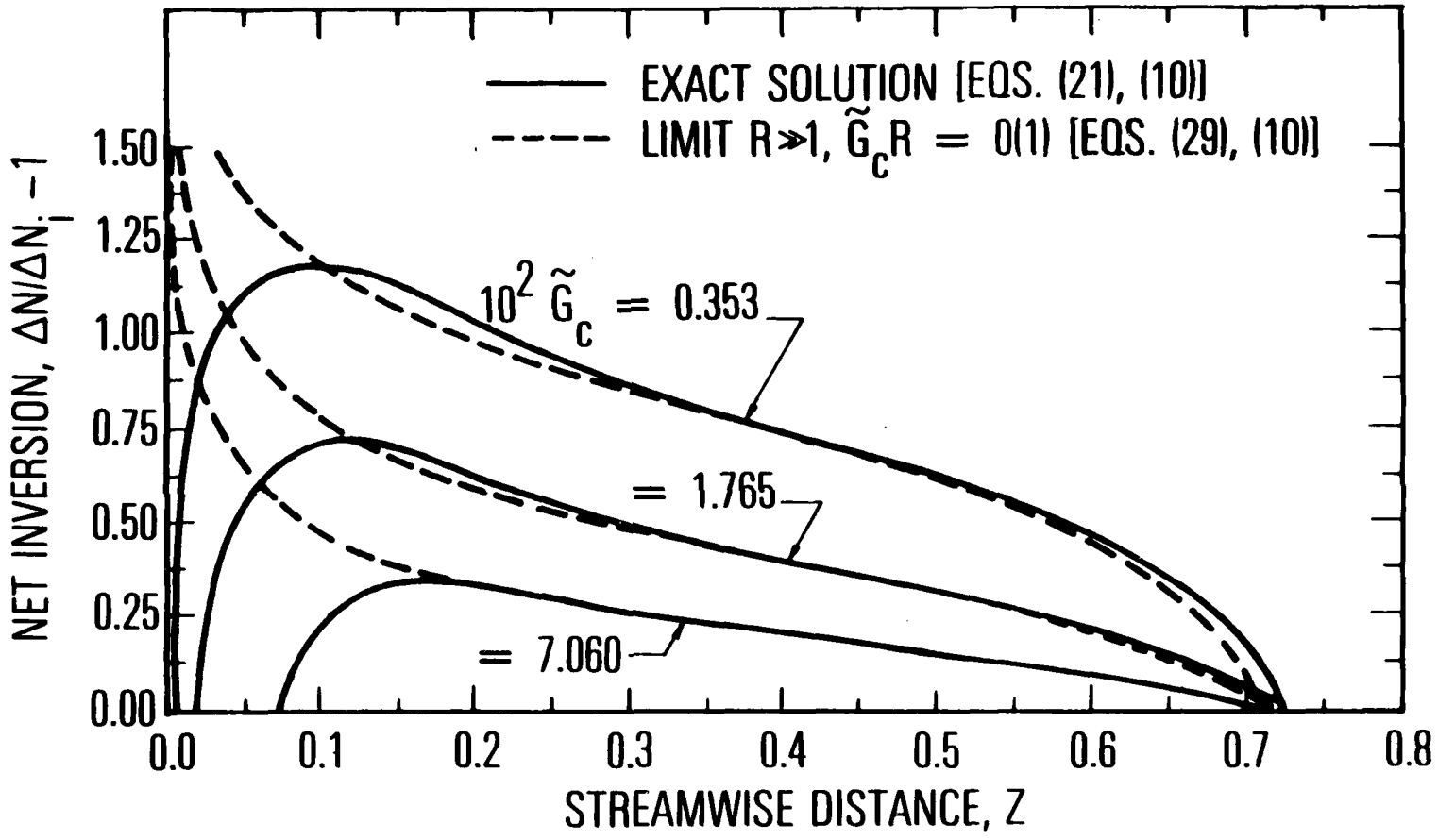

Figure 7(b). Numerical solution of Eqs. (10), (21), and (24) for case of laminar flame sheet R = 100, X_e = 0.001, and $10^2\,\tilde{G}_c$ = 0.353, 1.765, 7.060, including comparison with analytic solution in limit R >> 1, R $\tilde{G}_c$ = O(1); net inversion, $\Delta N/\Delta N_i$

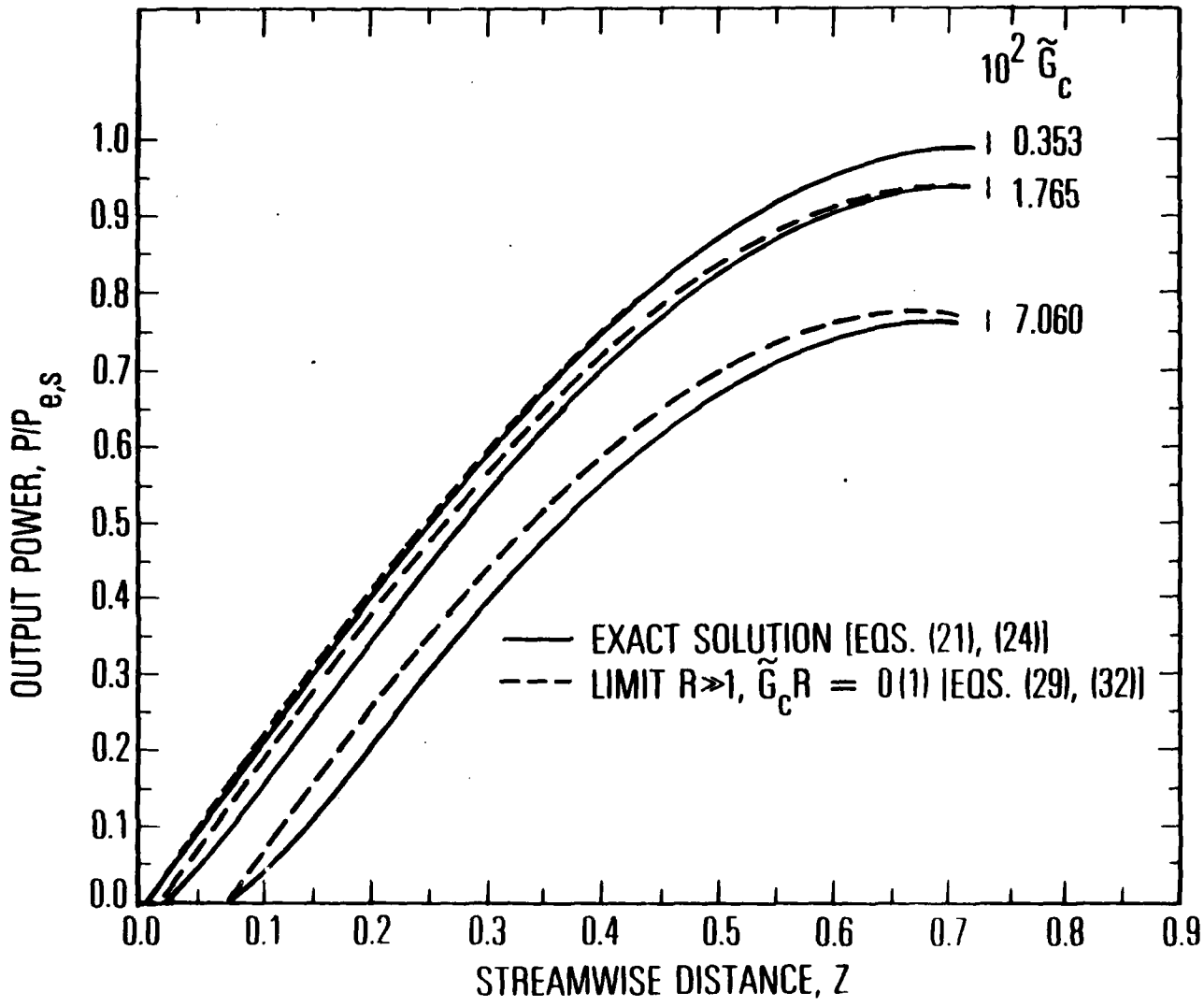

Figure 7(c). Numerical solution of Eqs. (10), (21), and (24) for case of laminar flame sheet R = 100, X_e = 0.001, and $10^2\,\tilde{G}_c$ = 0.353, 1.765, 7.060, including comparison with analytic solution in limit R >> 1, R $\tilde{G}_c$ = 0(1); output power $P_e/P_{e,s}$

Substitution of the identity

$$1 - H(X_f,X_e)\ F(X_f,X_e) = \frac{4e^{-X_e^2}}{3\pi^{1/2}}\ X_f^3\left[1 + O(X_f^2)\right] \tag{25}$$

into Eq. (21a) indicates RX_f^3 is of the order 1 in the present approximation. Neglect of terms of the order X_f^2 compared with 1 in Eq. (21a) indicates that the derivative term is negligible therein. Equation (21a) becomes

$$X_f^3 = \frac{3}{4}\ \frac{\pi^{1/2}}{\tilde{G}_c R}\ e^{X_e^2}\left(\frac{1}{2Z} - Z - \tilde{G}_c\right)\left[1 + O(X_f^2)\right] \tag{26a}$$

Other quantities of interest are

$$\frac{\Delta N}{\Delta N_i} = 1 + \frac{e^{-X_e^2}\ X_f^2}{F(0,X_e)} - \frac{4}{3\pi^{1/2}}\ e^{-X_e^2}\ X_f^3 + O\left(X_f^4\right) \tag{26b}$$

$$\pi\ \Delta\nu_h\ \tilde{G}_c\ \tilde{I} = \frac{\tilde{G}_c\ R\ e^{-X_e^2}}{F(0,X_e)}\left(X_f^2 - X^2\right)\left[1 + O\left(X_f^2\right)\right] \tag{26c}$$

$$2\ \zeta_D^{1/2}\ \frac{dP}{dZ} = 1 - 2Z^2 - 2\ \tilde{G}_c\ Z\left[1 + O(X_f^2)\right] \tag{26d}$$

$$2\ \zeta_D^{1/2}\ P = \left\{Z - \frac{2}{3}\ Z^3 - \tilde{G}_c\ Z^2\left[1 + O\left(X_f^2\right)\right]\right\}_{Z_i}^{Z} \tag{26e}$$

The station Z_e at which $dP/dZ = 0$ is

$$Z_e = [(2 + \tilde{G}_c^2)^{1/2} - \tilde{G}_c]/2 \tag{27}$$

Net output power is obtained by using Z_e as the upper limit in Eq. (26e).

Results for a saturated laser can be obtained by considering the limit $R \to \infty$, $\tilde{G}_c \to 0$, $R\tilde{G}_c \gg 1$. It is found that

$$Z_i = 0 \qquad Z_e = 1/2^{1/2} \tag{28a}$$

$$2\,\zeta_D^{1/2}\,P_{e,s} = 2^{1/2}/3 \tag{28b}$$

where $P_{e,s}$ denotes net saturated output power and is a convenient reference.

In the present limit, the dependent variables X_f, $\Delta N/\Delta N_i$, and $\tilde{G}_c\,\tilde{I}$ depend on Z, X_e, and $\tilde{G}_c R$. The parameters Z_i, Z_e, and $\zeta_D^{1/2} P_e$ depend only on $\tilde{G}_c$. The medium acts like a homogeneously broadened medium, i.e., $X_f \to 0$, and lasing occurs at line center. Equations (26b) and (26c) are the same as those obtained for a homogeneous medium with lasing at line center and with zero power line center gain reduced by the factor $F(0,X_e)$ to account for the effect of spreading.

4. LIMIT $R \gg 1$, $R\tilde{G}_c = O(1)$

The present limit $R \gg 1$, $R\tilde{G}_c = (1)$ implies $\tilde{G}_c \ll 1$ and, therefore, implies a saturated laser. Moreover, because of the conflicting influence of R and $\tilde{G}_c$ on X_f, the limit $R\tilde{G}_c = O(1)$ ensures that X_f is of order 1.

If terms of the order $\tilde{G}_c$ and R^{-1} are neglected, the derivative term in eq. (21a) is again negligible, and Eq. (21a) becomes

$$Z = [(2 + \beta^2)^{1/2} - \beta]/2 \tag{29a}$$

where

$$\beta = \tilde{G}_c \, R \, [1 - F(X_f, X_e) \, H(X_f, X_e)] \, F(0, X_e)/F(X_f, X_e) \tag{29b}$$

An implicit solution for X_f in terms of Z is provided in Eq. (29). It is found that X_f decreases monatomically as Z increases from Z = 0 to Z = $1/\sqrt{2}$. In the vicinity of Z = 0 and Z = $1/\sqrt{2}$, respectively,

$$X_f^2 = (-1) \, \ln \, [2F(0, X_e) \, \tilde{G}_c \, RZ] \tag{30a}$$

$$X_f^3 = \frac{3\pi^{1/2}}{2} \, \frac{e^{X_e^2}}{\tilde{G}_c R} \left(\frac{1}{2^{1/2}} - Z \right) \left[1 + O(X_f^2) \right] \tag{30b}$$

Thus, $X_f \to \infty$ as $Z \to 0$, and $X_f \to 0$ as $Z \to 1/\sqrt{2}$. The derivative dX_f/dZ becomes infinite as $Z \to 0$ and as $Z \to 1/\sqrt{2}$, and, therefore, should be retained in Eq. (21a) when these regions are considered. Lasing is initiated at station $Z_i = \tilde{G}_c \ll 1$. The boundary condition $X_f = 0$ at Z_i is not satisfied because of neglect of the derivative term in Eq. (21). Lasing intensity is found from

$$\pi \, \Delta\nu_h \, \tilde{G}_c \, \tilde{I} = \tilde{G}_c \, R \left[\frac{F(X, X_e)}{F(X_f, X_e)} - 1 \right] \tag{31}$$

The intensity is proportional to zero power lineshape, and $\tilde{I} \to 0$ as $X \to X_f$. Since $\tilde{G}_c \ll 1$, the laser is saturated and output power is obtained from Eqs. (28a) and (28b). Equations (28), (30), and (31) indicate that X_f, dP/dZ, and $\tilde{I}$ all become zero at $Z = 1/\sqrt{2}$. In more general cases, neither X_f nor $\tilde{I}$ is zero at the station where $dP/dZ = 0$ (i.e., at Z_e).

In the present limit, the variables X_f, $\Delta N/\Delta N_i$, and $\tilde{G}_c\,\tilde{I}$ depend on Z, X_e, and $\tilde{G}_c R$. The quantities Z_i, Z_e, and $\zeta_D^{1/2}\,P_e$, however, are constants in the limit $\tilde{G}_c \ll 1$.

An improved estimate for output power can be obtained by using a mean value for $H(X_f, X_e)$ in the integral of Eq. (24). The result can be expressed

$$\frac{P}{P_{e,s}} = \frac{3}{2^{1/2}} \left\{ Z - \frac{2}{3} Z^3 - \tilde{G}_c Z^2 + 0\left[\tilde{G}_c \left(\frac{\Delta N}{\Delta N_i} - 1\right)\right] \right\}_{Z_i}^{Z} \tag{32}$$

where the error term tends to become small as $Z \to Z_e$ (e.g., Fig. 7). Net output power is obtained by utilizing Z_e from Eq. (27) as the upper limit in Eq. (32). Equation (32) is equivalent to Eq. (26e), and both provide accurate estimates of laser output power for $R \gg 1$.

III. RESULTS AND DISCUSSION

In a typical cw chemical laser,[3] $R = 0(10) - 0(100)$ and $\tilde{G}_c = 0(0.01)$. Hence, the limiting solutions in Sections II.C.3 and II.C.4 include most cases of practical interest. The intensity $\tilde{I}$ is positive for all values of ζ and X_f, and, therefore, these limiting solutions are physically realistic. The negative values of $\tilde{I}$ encountered at lower values of R can be avoided if the lineshape in region $|X/X_f| > 1$ is not specified a priori. The regime where negative values of $\tilde{I}$ occur is of less interest, and realistic solutions for this regime are not pursued herein.

Numerical results have been obtained for the case of a laminar flame sheet [Eqs. (10), (21), and (24)]. Parameters in the range $0.00353 \leq (2/\pi)\zeta_D^{1/2} G_c \leq 0.0706$, $0.001 \leq X_e \leq 2.5$, and $1 \leq R \leq \infty$ were considered. The first of these inequalities corresponds to $0.01 \leq (g_c)_{av}/g_{mzp} \leq 0.2$ [Eq. (19)]. Results are presented in Tables I through III and Figs. 5 through 7.

In Table I, the values of Z_i at which lasing is initiated are indicated. These are independent of R and increase as X_e and G_c increase. In Table II is presented the station Z_e at which $dP/dZ = 0$ and the corresponding output power P_e normalized to the saturated laser output power $P_{e,s}$. The ratio $P_e/P_{e,s}$ decreases as X_e and G_c increase and is relatively insensitive to R for $R > 0$ (10); therefore, Eq. (26e) provides the output power for cases of practical interest. The results for $R = 100$ are also indicated in Fig. 5. The downstream station at which $X_f = 0$ is denoted Z_L. Values of Z_L and the corresponding output power P_L are indicated in Table III. The values of P_L depart significantly from the corresponding values of P_e in Table II only for $R = 1$. The difference is the result of negative values of $\tilde{I}$. Thus, the data of Table III illustrate the nature of the present solution for $R = 0(1)$ and are primarily of academic interest.

The variation of X_f, ΔN, and P with Z is indicated in Fig. 6 for R = 1.0, X_e = 0.001, and several values of G_c. Results from the numerical integration of Eq. (21) for R = 100 are compared with results from the limiting solution of Section II.C.4 in Fig. 7. The agreement is good except for points in the vicinity of Z_i and Z_e where poor agreement is expected because of neglect of the derivative term in the limiting solution.

IV. CONCLUDING REMARKS

In Table II laser output power is demonstrated to depend primarily on $\tilde{G}_c$ and X_e and to be relatively independent of variations in R for the practical range $R > O(10)$. Hence, solutions in the limit $R \to \infty$ provide useful estimates for the effect of gain saturation $\tilde{G}_c$ and source flow X_e on the output power from multiple longitudinal mode cw chemical lasers.

A number of complex multitransition-multichemical reaction numerical codes have been developed (e.g., Ref. 8) that can be used to evaluate cw chemical laser performance with the assumption of a single longitudinal mode at line center for each lasing transition. In the present model, $X_f \to 0$ as $R \to \infty$, i.e., the limit $R \to \infty$ corresponds to a single longitudinal mode at line center. Therefore, numerical codes in which this assumption is made provide reasonable estimates for the effect of gain saturation and source flow on multiple longitudinal mode cw chemical laser output power if the correct zero power line center gain is used [Eq. (5)], and the conditions in Eqs. (1a) and (1b) are satisfied.

It is also seen, from Fig. 7, that the limit solution $R \gg 1$ and $\tilde{G}_c R = O(1)$ provides reasonably accurate simple-closed-form analytic expressions for laser performance in the regime of interest.

REFERENCES

1. Bennett, W. R., Jr., "Hole Burning Effects in a HeNe Optical Maser," Phys. Rev. 126, 580 (1961).

2. Sargent, M., II, Scully, M. O., and Lamb, W. E., Jr., Laser Physics, Addison-Wesley, Reading, Mass., (1974), pp. 144-155.

3. Mirels, H., "Inhomogeneous Broadening Effects in CW Chemical Lasers," AIAA J. 17, 478 (1979).

4. Mirels, H., "Inhomogeneous Broadening Effects in Multimode CW Chemical Lasers," Appl. Opt. 20, 362 (1981).

5. Bullock, D. L., and Lipkis, R. S., "Saturation of the Gain and Resonant Dispersion in Chemical Lasers," presented at Fourth Annual Tri-Service Chemical Laser Conference, Albuquerque, N.M., 22 August 1979.

6. Livingstone, P.M., and Bullock, D. L., "Line-shape Flattening Resulting from Hypersonic Nozzle Wedge Flow in Low-Pressure Chemical Laser," Opt. Lett., 5, 291 (1980).

7. Mirels, H., "Source Flow Effect on Lineshape," Appl. Opt. 20, 835 (1981).

8. Sentman, L. H., "Chemical Laser Power Spectral Performance: A Coupled Fluid Dynamics, Kinetic and Physical Optics Model," Appl. Opt. 17, 2244 (1978).

SYMBOLS

a	Most probable particle thermal speed
$D(\ )$	Dawson integral, Eq. (17)
$F(X,X_e)$	Zero power lineshape, Eq. (5)
$G(\nu)$, G_c	Normalized gain and threshold gain, Eqs. (4a) and (7a)
$\tilde{G}_c$	Threshold gain parameter, Eq. (20)
$g(\nu)$	Small signal gain, Eq. (4)
g_c, g_{mzp}	Threshold gain, maximum zero power gain, Eqs. (7b) and (19)
$H(X_f,X_e)$	Net inversion $\Delta N/\Delta N_{\nu_i}$, Eq. (10)
$I_j, \tilde{I}(\nu)$	Lasing intensity, Eq. (11)
j	Longitudinal mode index
k_{cd}, k_{cr}	Collisional deactivation and cross relaxation (molecular collision) rates, sec^{-1}
L	Mirror separation
N, N_1, N_2, N_T	Normalized population density, Eqs. (2), (11), and (16)
$N(\nu), N_\nu$	Normalized population in frequency interval ν to $\nu + d\nu$, Eq. (2)
$\Delta N, \Delta N_\nu$	Normalized population difference, Eq. (2)
$n, n(\nu)$	Population density, Eq. (2)
n_{sc}	Number of semichannels, Fig. 1
P, P_e	Output power liberated up to station ζ, ζ_e, Eq. (11)
$P_{e,s}$	Output power for saturated laser, Eq. (28)
$\bar{p}_o$	Reciprocal of Doppler width, Eq. (2)
R	k_{cr}/k_{cd}

u	Velocity in x direction, Fig. 1
V_e	Transverse velocity at edge of source flow, Fig. 3
w	Channel semiwidth, Fig. 1
X	Normalized frequency, Eq. (5)
X_e	Source flow parameter, V_e/a
X_f	Value of X corresponding to largest lasing frequency
x,y	Streamwise and lateral distance, Fig. 1
x_D	Characteristic diffusion distance, Fig. 1
$y_f(x)$	Flame sheet location, Fig. 1
ζ,ζ_D	Normalized streamwise distance, $k_{cd}x/u$, $k_{cd}x_D/u$
ν	Frequency, sec^{-1}
$\Delta\nu_c,\Delta\nu_d,\Delta\nu_h$	Characteristic frequencies, Eq. (1)
σ	Stimulated emission cross section, Eq. (4)

Subscripts

o	Line center value
1,2	Levels 1 and 2
av	Average value, Eq. (4)
c	Related to cavity
e	End of positive lasing region (station at which $dP/d\zeta = 0$)
f	Associated with final (highest) lasing frequency
i	Value at start of lasing
j	Longitudinal mode index

L	Downstream station at which $X_f = o$
ν	Pertaining to frequency ν
ν_f	Pertaining to highest lasing frequency

LABORATORY OPERATIONS

The Laboratory Operations of The Aerospace Corporation is conducting experimental and theoretical investigations necessary for the evaluation and application of scientific advances to new military space systems. Versatility and flexibility have been developed to a high degree by the laboratory personnel in dealing with the many problems encountered in the nation's rapidly developing space systems. Expertise in the latest scientific developments is vital to the accomplishment of tasks related to these problems. The laboratories that contribute to this research are:

Aerophysics Laboratory: Launch vehicle and reentry aerodynamics and heat transfer, propulsion chemistry and fluid mechanics, structural mechanics, flight dynamics; high-temperature thermomechanics, gas kinetics and radiation; research in environmental chemistry and contamination; cw and pulsed chemical laser development including chemical kinetics, spectroscopy, optical resonators and beam pointing, atmospheric propagation, laser effects and countermeasures.

Chemistry and Physics Laboratory: Atmospheric chemical reactions, atmospheric optics, light scattering, state-specific chemical reactions and radiation transport in rocket plumes, applied laser spectroscopy, laser chemistry, battery electrochemistry, space vacuum and radiation effects on materials, lubrication and surface phenomena, thermionic emission, photosensitive materials and detectors, atomic frequency standards, and bioenvironmental research and monitoring.

Electronics Research Laboratory: Microelectronics, GaAs low-noise and power devices, semiconductor lasers, electromagnetic and optical propagation phenomena, quantum electronics, laser communications, lidar, and electro-optics; communication sciences, applied electronics, semiconductor crystal and device physics, radiometric imaging; millimeter-wave and microwave technology.

Information Sciences Research Office: Program verification, program translation, performance-sensitive system design, distributed architectures for spaceborne computers, fault-tolerant computer systems, artificial intelligence, and microelectronics applications.

Materials Sciences Laboratory: Development of new materials: metal matrix composites, polymers, and new forms of carbon; component failure analysis and reliability; fracture mechanics and stress corrosion; evaluation of materials in space environment; materials performance in space transportation systems; analysis of systems vulnerability and survivability in enemy-induced environments.

Space Sciences Laboratory: Atmospheric and ionospheric physics, radiation from the atmosphere, density and composition of the upper atmosphere, aurorae and airglow; magnetospheric physics, cosmic rays, generation and propagation of plasma waves in the magnetosphere; solar physics, infrared astronomy; the effects of nuclear explosions, magnetic storms, and solar activity on the earth's atmosphere, ionosphere, and magnetosphere; the effects of optical, electromagnetic, and particulate radiations in space on space systems.

. . .